International Journal of Engineering

Journal Homepage: www.ije.ir

Corrosion Polarization Behavior of Al-SiO_2 Composites in 1M and Related Microstructural Analysis

N. Munasir*[a], Triwikantoro[b], M. Zainuri[b], R. Bäßler[c], Darminto[b]

[a] *Department of Physics, Faculty of Mathematics and Sciences, Universitas Negeri Surabaya, Jl. Ketintang Surabaya, Indonesia*
[b] *Department of Physics, Faculty of Sciences, Institut Teknologi Sepuluh Nopember (ITS), Surabaya, Indonesia*
[c] *BAM-Federal Institute for Materials Research and Testing, Division 6.2: Corrosion Protection of Technical Plants and Equipment, Unter den Eichen, Berlin, Germany*

P A P E R I N F O

Paper history:
Received 13 February 2019
Received in revised form 29 April 2019
Accepted 03 May 2019

Keywords:
Al-Composite
Corrosion
Corrosion rate
SiO_2 Nanoparticle
Tafel Plot

A B S T R A C T

The composites combining aluminum and silica nanoparticles with the addition of tetramethylammonium hydroxide (Al-SiO_2(T)) and butanol (Al-SiO_2(B)) as mixing media have been successfully fabricated. Corrosion behavior of Al-SiO_2 composites before and after exposure in 1M NaCl solution was examined using potentiodynamic polarization (Tafel curve analysis). The study was also equipped with scanning electron microscopy (SEM), energy dispersive X-ray (EDX), and X-ray diffraction (XRD) investigations. Before exposure, Al-SiO_2(T) exhibited the best corrosion resistance. Performance improvement was indicated by Al-SiO_2(B) up to 10 times better than Al-SiO_2(T) after exposure. The increased SiO_2 content did not significantly enhance the corrosion resistance of the composites. The Al-SiO_2 composites with 5% SiO_2 content showed very high corrosion resistance (as the optimum composition). Furthermore, pitting corrosion was observed in the Al-SiO_2 composites, indicated by the formation of corrosion products at grain boundaries. The product was affected by the presence of SiO_2 in the Al matrix and the NaCl environment at 90°C (approach to synthetic geothermal media: Na^+, Cl, H^+, OH^-). Our study revealed the presence of γ-Al_2O_3, γ-$Al(OH)_3$, and $Al(OH)_2Cl$ as the dominant corrosion products.

***doi**: 10.5829/ije.2019.32.07a.11*

NOMENCLATURE

$At\%$	Atomic percent	I_{corr}	Corrosion current (A)
β_a	Tafel anodic coefficient	J_{corr}	Corrosion current density (A/cm^2)
β_c	Tafel cathodic coefficient	R_p	Polarization resistance (Ohm.cm^2)
C	Constant of corrosion rate unit divided by the specimen density and area	W_{eq}	The equivalent weight of material investigated
CR	Corrosion rate (*mmpy*)	$Wt\%$	Atomic Weight percent
E_{corr}	Corrosion potential (Volt)	V_{corr}	Corrosion rate (*mmpy*)

1. INTRODUCTION

Aluminum is one of the most popular non-ferrous metals used as a matrix in metal-matrix composites (MMCs), because of its low density and its highly resistant to corrosion due to the existence of a thin layer of oxide on its surface, formed by oxidation with oxygen in the air [1]. The introduction of other elements/ compounds into the aluminum matrix has promoted to improvements of MMCs' properties, providing materials for wide range applications; such as for automobiles, aircraft, ships, and energy sectors [1, 2]. Aluminum and its alloys are widely used in a large

*Corresponding Author Email: *munasir_physics@unesa.ac.id* (N. Munasir)

Please cite this article as: N. Munasir, Triwikantoro, M. Zainuri, R. Bäßler, Darminto, Corrosion Polarization Behavior of Al-SiO_2 Composites in NaCl 1M and Related Microstructural Analysis, International Journal of Engineering (IJE), IJE TRANSACTIONS A: Basics Vol. 32, No. 7, (July 2019) 982-990

number of industrial applications due to their excellent combination of properties, e.g., good corrosion resistance, excellent thermal conductivity, high strength to weight ratio, easy to deform, and high ductility [1–9].

In geothermal exploration, crust formation and corrosion that reduce turbine efficiency is one of the main problems during the geothermal energy production process. Common types of scales include calcium carbonate, silica, amorphous silicates, and mixtures of metal oxides and sulfides. Besides steam, the contaminants like sulfur, vanadium, and sodium are also emitted as products, which can react at high temperatures with air and water forming molten salts, which may probably accelerate corrosion of materials. Therefore, for high-temperature applications, materials with mechanical strength, high resistance to corrosion and oxidation are necessary to develop [2].

Studies on corrosion behavior of aluminum and its alloys [10–16] and aluminum matrix composites (AMCs) reinforced flay-ash [17], SiC [18, 19], Al_2O_3 [20], and graphite [21] in several media have been conducted. Corrosion behavior is not only measured using electrochemical impedance spectroscopy (EIS) but also by potentiodynamic polarization from Tafel polarization curve and Tafel impedance plots. Those studies focused on the type of corrosive media with various concentrations and temperatures. Common corrosion products in aluminum-based materials are galvanic corrosion, pitting corrosion, and grain boundaries corrosion [22, 23]. The galvanic and pitting corrosions occurred in Al-Gr composites, and it was revealed that the addition of Gr (1-3%wt) increased the corrosion rate of the Al-Gr composites [11]. In addition, the concentration and temperature of NaCl as the corrosion medium enhanced the corrosion rates of 6061-SiC [17] and 6063-Al_2O_3 [19].

To date, the influence of SiO_2 nanoparticles as filler in AMCs have been one of the most exciting topics explored by many researchers [1, 2, 7]. However, exploration is generally focused on mechanical characteristics. Some reports also explore the corrosion behavior of AMCs, particularly on the effect of chemical-based corrosion media. For example, Al-6030 exhibited lower pitting corrosion rate due to the increasing concentration and temperature of the corrosion media [19, 24, 25]. Salehi et al. claimed that silicon could be used to enhance the Al-Si corrosion rate in 3.5% NaCl medium because of the formation of Na_2SiO_3 in Al layers [26]. The higher NaCl concentration promoted the formation of roughness on the Al-Si composites [26]. The influence of SiC addition on Al-6061 alloy contributed to the increasing corrosion rate as the exposure time increased, but the corrosion rate decreases when the SiC particle size dropped to nano [27]. The addition of Al_2O_3 in Al-Cu-Mg Alloy decreased the pitting corrosion rate in seawater medium [28]. Like Gr, SiO_2 addition (1-3%wt) also took good control of the anti-corrosion characteristics of Al-Cu-Mg-SiO_2 composites in NaCl medium [29].

This study is aimed to investigate the corrosion behavior of Al-SiO_2 composites, with which SiO_2 nanoparticle as the reinforcement in Al matrix, before and after exposure in 1M NaCl solution using potentiodynamic test and Tafel polarization curve techniques by evaluating the corrosion rate and electrochemical processes for the formation of corrosion products using transition state theory. Furthermore, the type of corrosion and its product will be inspected using SEM-EDX and XRD.

2. EXPERIMENTAL

2. 1. Materials Merck KgaA, Frankfurter, Germany supplied high purity aluminum powder (> 90%). Silica (SiO_2) powder with an average particle size of ~35 nm [30]. The Al-SiO_2 composites were produced via a powder metallurgical technique. Volume fraction of SiO_2 was varied at 5, 10, 15, 20, 25, and 30% [31]. The SiO_2 was dispersed in tetramethyl-ammonium hydroxide (TMAH) and butanol [31]. The green samples were heated to 200°C for 45 minutes until the condensation in the upper part of the glass tube has disappeared, the vacuum was applied, and the temperature was increased to 500°C for two hours. To prevent the possible overrun of the designated temperature, the heating process was split into incremental steps. The heating rate of 3°C/min was used upto 480°C and changed to 1°C/min for the temperature range 480-500°C. This heating rate was also applied while keeping the sample at 500 °C. Fluctuations of around 5 °C were observed. After two hours, the specimen was cooled down in a furnace overnight.

2. 2. Characterization

2. 2. 1. Electrochemical Test Corrosion behavior test of Al-SiO_2 composites was done using potentiodynamic polarization. The potentiodynamic polarization was composed of stainless steel counter electrode, Al-SiO_2 working electrode, and Ag/AgCl reference electrode. The measurement was run with applied potential from -0.3 V to +0.3 V at a scan rate of 2 mV/s. The potentiodynamic polarization outputs are current-voltage (I-V) curve and corrosions parameters β_a, β_c, R_P, J_{corr}, I_{corr}, $E_{corr,}$ and V_{corr}. Meanwhile, the cyclic voltammetry test was performed by 797 Computrance with Pt working electrode and Ag/AgCl reference electrode.

The samples were exposed to 1M NaCl environment for seven—days at temperatures of 90 °C. The measurement was conducted under initial sweep

potentials from -1.2 V to 1.2 V; with first and second vortexes, respectively, 1.0 V and -1.0 V at step potential 0.006 V and sweep rate 1.0 V/sec and 15 s time deposition.

2. 2. 2. Structural Investigation The scanning electron microscopy (SEM) and energy dispersive X-ray (EDX) investigation were used to study the microstructure and elemental mapping of Al-SiO_2 composites. The SEM images were captured by using Inspect S50, XT microscope server integrated with FEI Software. All SEM/EDX data were collected under the same experimental conditions, high vacuum chamber pressure of 4.1×10^{-4} mBar, emission current of 0.1 µA, working distance range of 12 mm, and high voltage of 10 kV. The X-ray powder diffraction pattern of bulk Al-SiO_2 composites was collected by PAN-analytical diffractometer using monochromated CuKα radiation operating at 40kV/40mA. All XRD data were collected under the same experimental conditions, in the angular range $5° \leq 2\theta \leq 90°$ with a scan rate of 0.02 °/min at ambient condition.

3. RESULT AND DISCUSSION

3. 1. Polarization Linear Analysis Based on Tafel plots analysis from linear polarization test [32], V_{corr} can be obtained. Corrosion current density J_{corr} (A/cm^2) can be calculated using the Stern-Geary equation [33, 34]:

$$J_{corr} = \frac{\beta_a \beta_c}{2.303 R_p (\beta_a + \beta_c)} \quad (1)$$

where β_a is Tafel anodic coefficient, β_c Tafel cathodic coefficient, and R_p polarization resistance (ohm·cm^2). The Tafel coefficient is obtained from the gradient of the Tafel plot. The corrosion rate V_{corr} is given by [23, 32]:

$$V_{corr} = C \times J_{corr} \times W_{eq} \quad (2)$$

where C is a constant which labels the corrosion rate unit divided by the specimen density and area, and Weq is the equivalent weight of material investigated.

Polarization curves of non-exposed Al-SiO_2(T) and Al-SiO_2(B) are respectively given in Figures 1(a) and 1(b) with complete output analysis in Table 1. The analysis reveals that E_{ocp}, E_{corr}, E_{begin}, and E_{end} are different for every sample, followed by a change of I_{corr} and V_{corr} [17, 20]. Polarization resistant shows the degree of electron flow. Greater the polarization resistant indicates the lower corrosion rate.

Figure 2 shows the Tafel plots of Al-SiO_2(T) and Al-SiO_2(B) after exposure in 1M NaCl for 30 days at room temperature followed by seven days exposure at 90 °C. From Figure 2, the polarization cathodic lies between -0.4 V and 0.2V, and E_{cor} values are relatively close for all samples. The different trend of Tafel plots is observed for Al-SiO_2(T) and Al-SiO_2(B). From Figure 1(a), it is seen that the addition of SiO_2 causes an increase in both current and potential corrosion. Meanwhile, from Figure 1(b), ungradual change is not observed. Increasing the corrosion current implies decreasing polarization resistance, which means that the material will be easier to corrode or reduction of

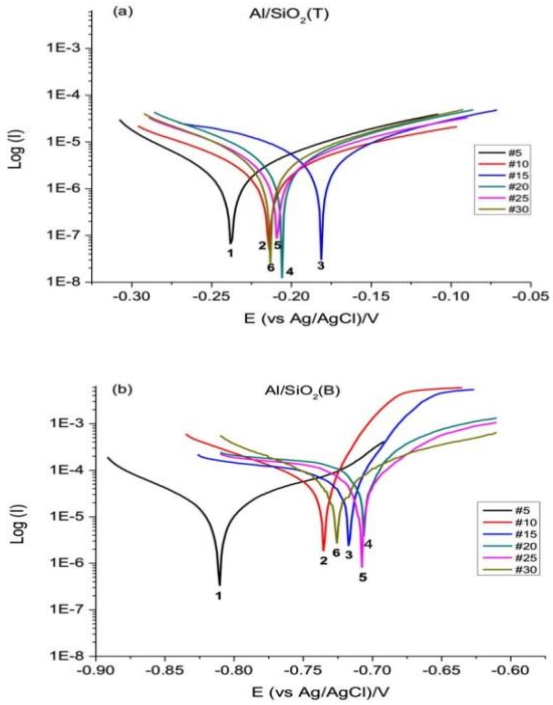

Figure 1. Tafel plots of (a) Al-SiO_2(T) and (b) Al-SiO_2(B) before exposure; #5, #10, #15, #20, #25 and #30 represent the values of SiO_2 volume fractions.

TABLE 1. Samples of Aluminum Reinforced SiO_2 NPs (Al-Composite)

No.	Volume Fraction of SiO_2 (x wt%)	Samples	
		Al-SiO2(B)	***Al-SiO2(T)***
1	0	#0B	#0T
2	5	#5B	#5T
3	10	#10B	#10T
4	15	#15B	#15T
5	20	#20B	#20T
6	25	#25B	#25T
7	30	#30B	#30T
	Corrosion Test	Before and after exposure *(in corrosive media)*	

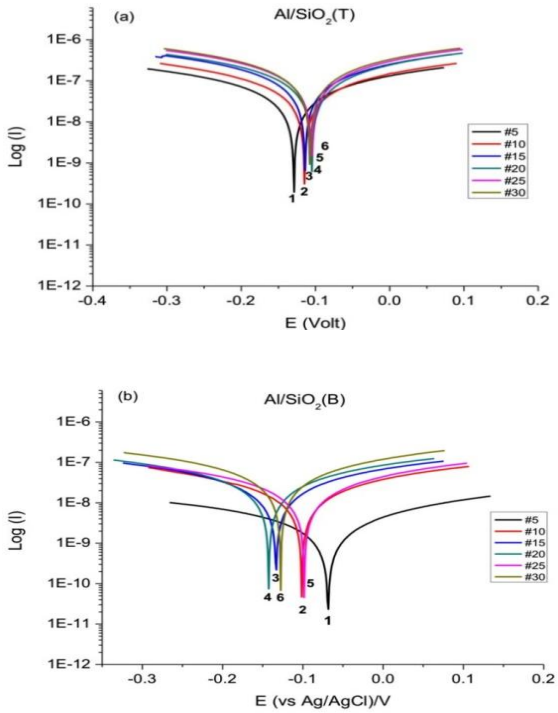

Figure 2. Tafel plots of (a) Al-SiO_2(T) and (b) Al-SiO_2(B) after exposure; #5, #10, #15, #20, #25 and #30 represent the values of SiO_2 volume fractions.

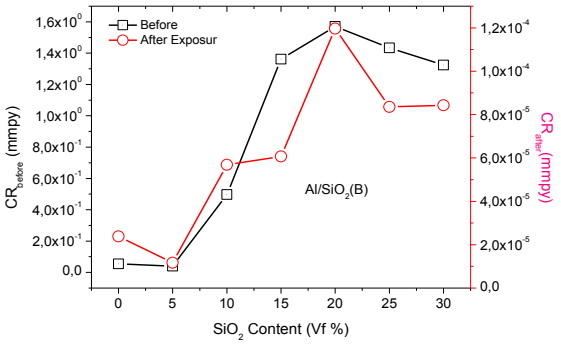

Figure 3. Corrosion rates of Al-SiO_2(B): before and after exposure in 1M NaCl environment

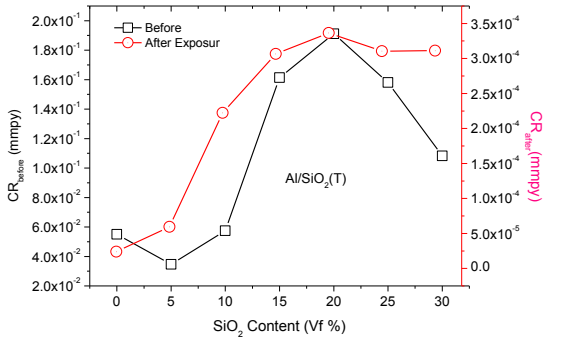

Figure 4. Corrosion rates of Al-SiO_2(T): before and after exposure in 1M NaCl environment

corrosion rate will appear. Furthermore, log *I* values of Al-SiO_2(T) are greater than that of Al-SiO_2(B). This result is in strong correlation with the previous result [34].

From polarization data, it canbe concluded that the addition of 5% SiO_2 promotes the lowest current density at 11.9100 nA/cm^2 and 1.0067 nA/cm^2 for Al-SiO_2(T) and Al-SiO_2(B), Respectively. On the othe hand, the addition of 20% SiO_2 exhibits the highest current density having values of 11.9100 nA/cm^2 and 1.0067 nA/cm^2 for Al-SiO_2(T) and Al-SiO_2(B), respectively. Figures 3 and 4 give the corrosion rates for non-exposed and exposed Al-SiO_2. The same trend of increasing corrosion rates is observed in Figure 3. However, the corrosion rates of non-exposed samples are lower than those of the exposed samples. The corrosion rates are in order of ~10^{-2} mm/y and ~10^{-5} mm/y for non-exposed and exposed samples, respectively.

The corrosion rates of the Al-SiO_2 composites is lower than that of unreinforced Al (the corrosion rate of Al is 0.055042 mm/y). From this experiment, the corrosion rates of non-exposed Al-SiO_2(T) and Al-SiO_2(B) are respectively 0.034618 mm/y and 0.039680 mm/y; and the corrosion rates of exposed Al-SiO_2(T) and Al-SiO_2(B) are 0.000059512 mm/y and 0.000011698 mm/y, respectively. The highest corrosion rate is found in 20% SiO_2 content, i.e. 0.19117 mm/y and 1.5700 mm/y for non-exposed Al-SiO_2 (B) and Al-SiO_2(T), respectively and 0.00036469 mm/y and 0.00011964 mm/y for exposed Al-SiO_2(B) and Al-SiO_2(T), respectively.

From another point of view, Figure 4 indicates that the Al-SiO_2(T) shows lower corrosion rates than the Al-SiO_2(B) (before exposure). After exposure, the Al-SiO_2(T) shows higher corrosion rates than the Al-SiO_2(B). It is, however, rather surprising that different mixing media (TMAH and butanol) plays an important role in corrosion behavior (in this case, corrosion rate) of the Al-SiO_2, before and after exposure. The Al-SiO_2(B) appears to be more resistive in corrosion than Al-SiO_2(T). It is predicted due to the scales formation (see sections 3.4 and 3.5) as a passivation layer which continues to occur even after exposure. The scale formation of Al-SiO_2(T) has completed before exposure, or during mixing and sintering processes [11, 35, 36].

3. 2. SEM/EDX Analysis The microstructural profile of corroded surface for sample #5B can be seen in Figure 5(a). The damage on the surface due to the exposure in the corrosive medium is seen sporadically in sample #5B. This evidence is revealed by mapping result on the whole observed surface, see Figure 5(b), and by elemental analysis, as given in Figure 5(c). The detected elements on those surfaces as the corrosion

products are O, Na, Al, Si, and Cl. Figure 5, magnification of 1000 × (100 µm in scale) does not reveal any damage on the surface, however, when the magnification of SEM was set to 70,000 × (1µm in scale), we could observe the damage along the grain boundaries as the consequence of corrosion (Figure 6(b)). From Figure 6, magnification of 1000 × (100 µm in scale) does not reveal any damage on the surface, however, when the magnification of SEM was set to 70,000 × (1µm in scale), we could observe the damage along the grain boundaries as the consequence of corrosion (Figure. 6(b))

The microstructural profile of corroded surface for sample #5B can be seen in Figure 5(a). The damage on the surface due to the exposure in the corrosive medium is seen sporadically in sample #5B. This evidence is revealed by mapping result on the whole observed surface, see Figure 5(b), and by elemental analysis, as given in Figure 5(c). The detected elements on those surfaces as the corrosion products are O, Na, Al, Si, and Cl. From Figure 5, magnification of 1000 × (100 µm in scale) does not reveal any damage on the surface, however, when the magnification of SEM was set to 70,000 × (1µm in scale), we could observe the damage along the grain boundaries as the consequence of corrosion (Figure 6(b)). From Figure 6, magnification of 1000 × (100 µm in scale) does not reveal any damage on the surface, however, when the magnification of SEM was set to 70,000 × (1µm in scale), we could observe the damage along the grain boundaries as the consequence of corrosion (Figure. 6(b)).

As depicted form Figure 7, the micro-structural profile for sample #5T after exposure as well as its elemental mapping analysis can be perceived. The identified elements as the corrosion products in that sample are O, Na, Al, Si, and Cl. This information can be confirmed by the X-ray diffraction data as shown in Figure 8. The Na and Cl atoms are in accordance with $NaCl_{(s)}$ crystal, which is assumed likely to remain still in the sidelines of the corrosion products. Similarly, the O and Al atoms are conforming with the presence of Al_2O_3 [37].

Furthermore, Figures. 8(a) and 8(b) represent the surface microstructural profile for sample #5T. In Figure 8(a), the damage is observed even at 100× magnification (1000 µm in scale), but not as in Figure 8(b). Obvious damage is well noticed for all samples at 2000× magnification (scale of 50 µm) and 5000× magnification (20 µm in scale) as depicted in Figures 8(b) and 8(c). If a comparison is done to evaluate the degree of damages due to the exposure between sample #5B (Figure 5) and sample #5T (Figure 7), it is revealed that sample #5T has larger damage than sample #5B.

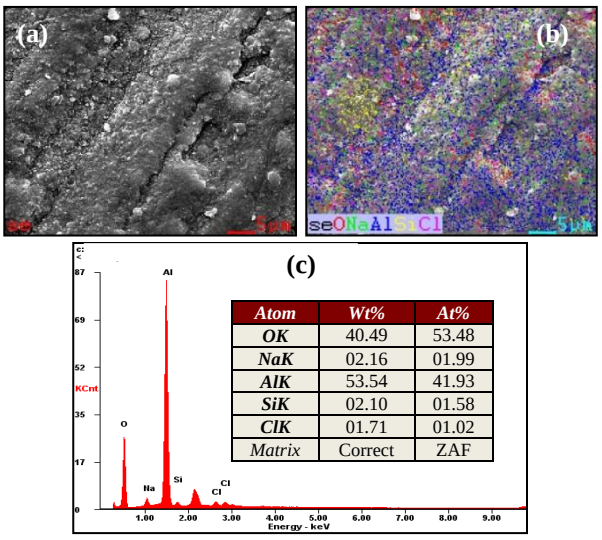

Figure 5. SEM-EDX analysis for Al-SiO_2 (#5B) composite after exposure: (a) SEM image, (b) elemental mapping, and (c) EDX spectra

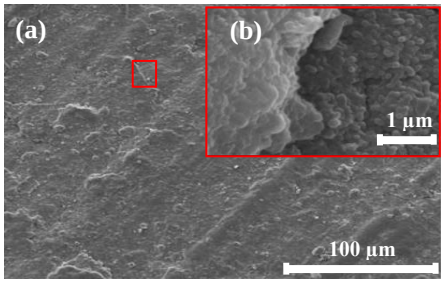

Figure 6. SEM photograph for Al-SiO_2 (#5B) composite after exposure: (a) at 1000× magnification, and (b) at 70.000× magnification

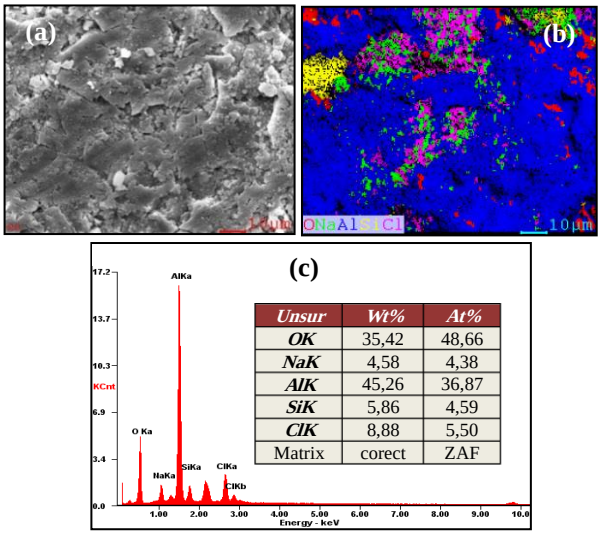

Figure 7. SEM photograph for Al-SiO_2 (#5T) composite after exposure: (a) SEM image, (b) elemental mapping, and (c) EDX spectra

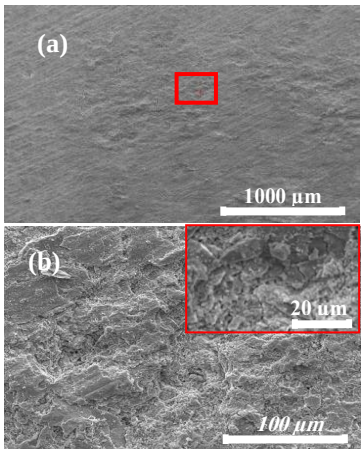

Figure 8. SEM photograph for Al-SiO_2 (#5T) composite after exposure with (a) 100× magnification, (b) 2000× magnification

3. 3. XRD Analysis Figure 9 represents the XRD profiles of unreinforced Al and Al-SiO_2 composites with 5% SiO_2 volume fraction. These XRD profiles are used to confirm the corrosion products of the composites and to explain the evidence of stronger corrosion resistance behavior of Al-SiO_2(B) rather than Al-SiO_2(T).

There is no other phase but aluminum in the unreinforced Al before exposure. Whereas after exposure, some XRD peaks that belong to alumina have appeared as the corrosion products. Introducing 5% SiO_2 volume fraction into the Al matrix promotes to the creation of new phases, γ-Al_2O_3, and γ-$Al(OH)_3$, due to the reaction of Al and SiO_2 in TMAH or butanol medium during the process. At this point, the X-ray diffraction peaks of SiO_2 cannot be detected since the crystalline state SiO_2 is amorphous. Besides that, the broader characteristic of XRD peaks of the composites is strongly predicted due to the contribution of amorphous SiO_2 nanoparticles. Notice from Figure 8 is that Al, γ-Al_2O_3, and γ-$Al(OH)_3$ phases are found in the composites. The presence of Al^{+3} ions forms $Al(OH)_3$, and $Al(OH)_2Cl$ (or $Al(OH)_2Cl_2$) and Al(OH) forms $Al(OH)_2Cl$ as the pitting corrosion product [12, 17, 21, 22, 34, 35]. Applying corrosion treatment to the unreinforced Al and the composites also cause background distortion of the XRD profiles, indicating that the NaCl medium may cause to crash the crystallines of the materials. Finally, the XRD characterization supports the SEM-EDX analysis.

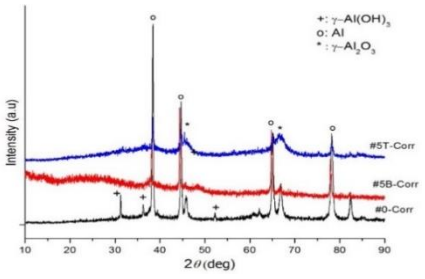

Figure 9. XRD patterns for unreinforced Al and Al-SiO_2 composites after exposure. The intensity is not to scale

The results of the analysis of corrosion rate performance as in Figure 10, this is the focus of analysis on the Tafel curve data for the first sample: #5B, #10B and #15B (Al-SiO_2 (B)) and the second sample: #5T, #10T and #15T (Al-SiO_2 (T)); there is a phenomenon, namely the position of E_{corr} that is far apart (~0.65 V), this scientific argument is supported by porosity data of Al-SiO_2 composite samples where both types of samples show the same pattern, whereas the fraction of volume (Vf%) SiO_2, porosity increases what happens to Al-SiO_2 composites actually increases, and in the composition of 5% SiO_2 the lowest porosity. And, if confirmed by SEM data it appears for the sample before exposure, it appears that on the surface of sample # 5, Al_2O_3 oxide layer has been formed compared to sample # 5B. This is thought to be the cause of Al-SiO_2(T) anti-corrosion performance compared to Al-SiO_2(B) [27].

Different things, it can be seen in Figure 11 that the data analysis on the Tafel curve for the Al-SiO2 sample (for 5%, 10% and 15% SiO2) after being exposed in 1M NaCl solution at 90°C, Ecorr position appears in both types of samples (Al-SiO_2 (B) and Al-SiO_2 (T) are more coincide than before exposure (Figure 10), and there is a shift in the potential position of the corrosion to the right. Example for sample # 5T before exposing Ecorr's position around -0.24Volt and after exposure around -0.13 Volt (shifting right as far as 0.11 Volt); and for sample #5B before exposing the E_{Corr} position around -0.82 Volt and after exposure around -0.08 Volt (shift right to ~ 0.74 Volt). Thus, based on the Tafel curve in Figures 10 and 11, the sample Al /SiO_2 (B) shifts further right from the sample Al /SiO_2 (T), so the potential for corrosion (E_{corr}) is more positive. The Ecorr potential position for the Al-SiO_2(T) (#5T, #10T and #15T) potential ranges lies in the potential range of the sample Al-SiO2 (b) which is located at a potential of -0.15 Volt to -0.075 volts. And for the corrosion current Icorr, the sample Al-SiO_2(T) shows a value of magnitude lower than the sample Al-SiO_2(T).

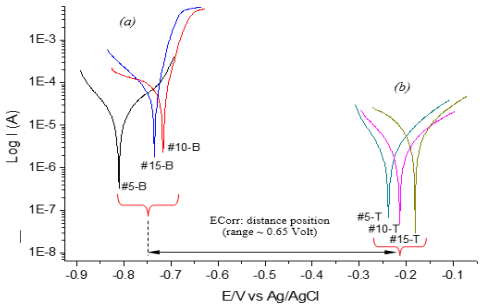

Figure 10. Tafel curve for samples before being exposed in 1M NaCl medium

Thus, the lower the I_{corr} position and the more positive the E_{corr}, the better the anti-corrosion performance will be. The sample Al-SiO_2(T) in the exposed state has a better anticorrosive performance than the Al /SiO_2(T) sample. The percentage of SiO_2 silica nano as a filler in aluminum Al /SiO_2 composites proved to influence its anti-corrosion performance, in addition to the active medium during the mixing process. In the composition of 5%, Al-SiO_2 composite SiO_2 has the best anti-corrosion performance in the exposure medium 1M NaCl solution at a temperature of 90°C (approach to the synthetic geothermal medium: Na^+, Cl^-, H^+, OH^-) [21, 38–40].

3. 4. Corrosion Mechanism in Al-SiO_2 Composites

The type of corrosion that often occurs in Al-based composites and Al-alloys is pitting corrosion. This type of corrosion is usually triggered by cracking or aggressive attacks from acidic ions from the environment. Besides that, the type of corrosion occurs due to the formation of potential differences between the grain boundaries inclusions of cathode and anode. If along the grain boundary area forms a semi-continuous network, intergranular corrosion or corrosion between crystals will occur. The precipitates can form intermetallic and cathodic intermetallic anodic [21].

Procedurally, the stages of the Al and Al-alloy corrosion mechanism are described as follows: the condition for corrosion: formation of anode and cathode potential, there is a corrosive trigger environment (dry electrochemical/oxidation), electron transfer from anode to cathode (internal metal properties), and charge transfer from metal surface to environment or vice versa, (ii) corrosion products in aluminium materials in aqueous medium (OH^-, H^+, Cl^-, etc.) include $Al(OH)_3$ and $Al(OH)_3Cl^-$, and (iii) the phenomenon of the formation of alumina oxide film (Al_2O_3) on the outer surface is naturally used as excellent anti-corrosion protector. The properties of Al_2O_3 are very hard, but not soluble in water. However, more acidic media (Cl^-, Na^+, and SO^{4-}) can destroy the alumina layers, and the corrosion process begins to occur. Illustration of the corrosion mechanism of Al-SiO_2 composites is presented in Figure 12.

Transfer of electrons from the anode in diffused metal towards the Al_2O_3 surface and interface area within the electrolyte promotes a double capacitance. On the surface of Al and Al-alloy, a huge number of micro galvanic cells are formed in such a way that the corrosion phenomenon can be modelled as alternating current electric circuits. The phenomenon of the load transfer rate and double-layer capacitors gives physical exposure to the amount of corrosion flow and corrosion potential (Tafel-plot). Disclosure and measurement of corrosion parameters are observed by relating the impedance and semi-circular curves of the corrosion resistance of the material to the corrosive medium, and the influence of the types of solutions and the addition of the type of load transfer inhibitor to the electrolyte solution. Also, there is an electron transfer from metal to the environment so that the metal oxidation number changes from zero to a specific positive number. There are interactions with electrons with atoms, ions or molecules during the oxidation and reduction processes. The corrosion profile of Al-SiO_2 composites in the NaCl medium at high temperatures (~ 90 °C) is given in Figure 13.

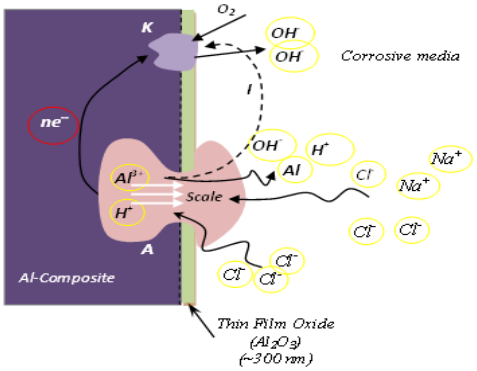

Figure 12. Pitting Corrosion Mechanism in Al-SiO_2 Composites

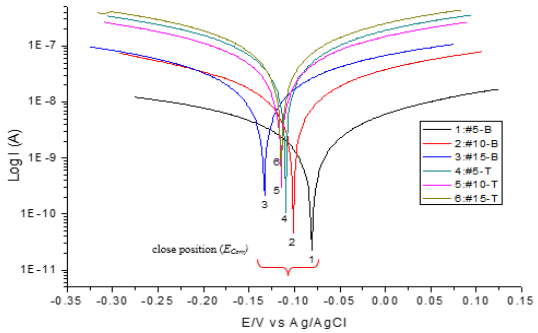

Figure 11. Tafel curves for samples that have been exposed in 1M NaCl the medium (at 90°C)

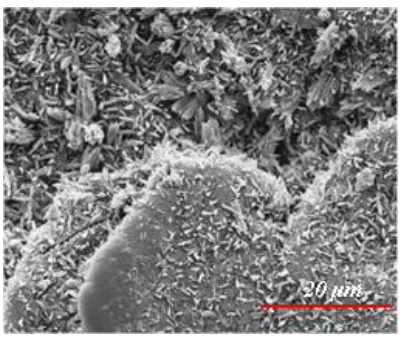

Figure 13. Corrosion Profile of Al-SiO_2 (#10B) before being exposed in 1M NaCl medium (T = 90 °C)

4. CONCLUSIONS

Corrosion behaviour of aluminum particulate composites containing 5, 10, 15, 20, 25, and 30 volume fraction silica in highly 1M NaCl saline solution (90°C, 7 days) reveals specific characteristics. Prior to exposure, Al-SiO_2(T) is more resistant to corrosion than Al-SiO_2(B), but after exposure in, Al-SiO_2(B) is ten times as strong as Al-SiO_2(T) to resist corrosion. Addition of SiO_2 volume fraction leads to decreasing corrosion resistance. The best performance of the composites as anti-corrosion is found in 5% SiO_2 content. Micrographic investigation shows that corrosion products are found in grain boundaries. The corrosion type of the composites in 1M NaCl environment is pitting corrosion. The corrosion products γ-Al_2O_3, γ-$Al(OH)_3$, and $Al(OH)_2Cl$ are due to the presence of SiO_2 in Al-SiO_2 composites and corrosive medium.

5. ACKNOWLEDGMENTS

One of the authors [M] is grateful to Universitas Negeri Surabaya (Unesa) and Institut Teknologi Sepuluh Nopember (ITS), which has supported the completion of this research. And gratefully for BAM Federal Institute for Materials Research and (division 6.2) Berlin-Germany, for his research visit.

6. REFERENCES

1. Rizkalla, H. L. and Abdulwahed, A., "Some mechanical properties of metal-nonmetal Al□SiO2 particulate composites", ***Journal of Materials Processing Technology***, Vol. 56, No. 1–4, (1996), 398–403.
2. Zuhailawati, H. and Samayamutthirian, P., "Fabrication of low cost of aluminium, matrix composite reinforced with silica sand", ***Journal of Physical Science***, Vol. 18, No. 1, (2007), 47–55.
3. Gregolin, E.N., Goldenstein, H., and Santos, R.G., "Co-continuous silica–aluminum composite", ***Journal of Materials Processing Technology***, Vol. 157–158, (2004), 688–694.
4. Gregolin, E.N., Goldenstein, H., Gonçalves, M.C., and Santos, R.G., "Aluminium Matrix Composites Reinforced with Co-continuous Interlaced Phases Aluminium-alumina Needles", ***Materials Research***, Vol. 5, No. 3, (2002), 337–342.
5. Gregolin, E.N., Button, S.T., Goldenstein, H., and Santos, R.G., "Hot Workability And Mechanical Properties Of An Aluminum-Silica Composite", In AMPT'01 – International Conference on Advances in Materials and Processing Technologies, Spain, (2001), 1–5.
6. Wang, J., "Mechanical alloying of amorphous Al–SiO2 powders", ***Journal of Alloys and Compounds***, Vol. 456, No. 1–2, (2008), 139–142.
7. Sayuti, M., Sulaiman, S., Vijayaram, T.R., Baharudin, B.T.H.T., and Arifi, M.K.A., "Manufacturing and Properties of Quartz (SiO2) Particulate Reinforced Al-11.8%Si Matrix Composites," In: Composites and Their Properties, InTech, (2012), 411–436.
8. Veeresh Kumar, G.B., P. Rao, C.S., Selvaraj, N., and Bhagyashekar, M.S., "Studies on Al6061-SiC and Al7075-Al 2 O 3 Metal Matrix Composites", ***Journal of Minerals and Materials Characterization and Engineering,*** Vol. 9, No.1, (2010), 43-55.
9. Hamouda, A.M.S., Sulaiman, S., Vijayaram, T.R., Sayuti, M., and Ahmad, M.H.M., "Processing and characterisation of particulate reinforced aluminium silicon matrix composite", ***Journal of Achievements of Materials and Manufacturing Engineering***, Vol. 25, No. 2, (2007), 11–16.
10. Banerjee, R., Panja, S., and Nandi, M., "An electrochemical and quantum chemical investigation of some corrosion inhibitors on aluminium alloy in 0.6 M aqueous sodium chloride solution", ***Indian Journal of Chemical Technology***, Vol. 18, No. 4, (2011), 309–313.
11. Sherif, E.S.M., "Corrosion and Corrosion Inhibition of Aluminum in Arabian Gulf Seawater and Sodium Chloride Solutions by 3-Amino-5-Mercapto-1, 2, 4-Triazole", ***International Journal of Electrochemical Science***, Vol. 6, (2011), 1479–1492.
12. Musa, A.Y., Mohamad, A.B., Kadhum, A.A.H., and Chee, E.P., "Galvanic Corrosion of Aluminum Alloy (Al2024) and Copper in 1.0 M Nitric Acid", ***International Journal of Electrochemical Science***, Vol. 6, No. 10, (2011), 5052–5065.
13. Sherif, E.S.M. and Park, S.M., "Effects of 1,4-naphthoquinone on aluminum corrosion in 0.50 M sodium chloride solutions", ***Electrochimica Acta***, Vol. 51, No. 7, (2006), 1313–1321.
14. Vrsalović, L., Kliškić, M., and Gudić, S., "Aplication of Phenolic Acids in the Corrosion Protection of Al- 0.8Mg Alloy in Chloride Solution", ***International Journal of Electrochemical Science***, Vol. 4, (2009), 1568–1582.
15. Liang, C.H. and Zhang, W., "Pitting Corrosion Mechanisms and Characteristics of Aluminum in Solar Heating Systems", ***Journal of the Chinese Chemical Society***, Vol. 53, No. 2, (2006), 313–318.
16. Bienia, J., Walczak, M., Surowska, B., and Sobczak, J., "Microstructure and corrosion behaviour of aluminum fly ash composites", ***Journal of Optoelectronics and Advanced Materials***, Vol. 5, No. 2, (2003), 493–502.
17. Pinto, G.M., Nayak, J., and Shetty, A.N., "Corrosion behaviour of 6061 Al-15vol. Pct. SiC composite and its base alloy in a mixture of 1: 1 Hydrochloric and sulphuric acid medium", ***International Journal of Electrochemical Science***, Vol. 4, No. 10, (2009), 1452–1468.
18. Escalera-Lozano, R. Gutiérrez, C.A., Pech-Canul, M.A., and Pech-Canul, M.I., "Corrosion characteristics of hybrid Al/SiCp/MgAl2O4 composites fabricated with fly ash and recycled aluminum", ***Materials Characterization***, Vol. 58, No. 10, (2007), 953–960.
19. Alaneme, K.K. and Bodunrin, M.O., "Corrosion behavior of alumina reinforced aluminium (6063) metal matrix composites", ***Journal of Minerals and Materials Characterization and Engineering***, Vol. 10, No. 12, (2011), 1153–1165.
20. Sherif, E.S.M., Almajid, A.A., Latif, F.H., and Junaedi, H., "Effects of Graphite on the Corrosion Behavior of Aluminum-Graphite Composite in Sodium Chloride Solutions", ***International Journal of Electrochemical Science***, Vol. 6, (2011), 1085–1099.
21. Gujarathi, K., "Corrosion of aluminum alloy 2024 belonging to the 1930s in seawater environment", Doctoral dissertation, Texas A&M University, (2008).
22. Szklarska-Smialowska, Z., "Pitting corrosion of aluminum", ***Corrosion Science***, Vol. 41, No. 9, (1999), 1743–1767.
23. Kan, H.M, Wang, Z.W., Wang, X.Y., and Zhang, N., "Electrochemical deposition of aluminum on W electrode from AlCl3-NaCl melts", ***Transactions of Nonferrous Metals Society of China***, Vol. 20, No. 1, (2010), 158–164.
24. Deepa, P. and Padmalatha, R., "Corrosion behaviour of 6063

aluminium alloy in acidic and in alkaline media", ***Arabian Journal of Chemistry***, Vol. 10, (2017), S2234–S2244.

25. Trdan, U. and Grum, J., "Investigation of Corrosion Behaviour of Aluminium Alloy Subjected to Laser Shock Peening without a Protective Coating", ***Advances in Materials Science and Engineering***, Vol. 2015, (2015), 1–9.
26. Salehi Doolabi, D., Ehteshamzadeh, M., and Asadi Zarch, M., "Microstructure and Corrosion Performance of Silica Coatings on Aluminum Surface Prepared by Plasma Electrolysis Technique", ***International Journal of Engineering - Transactions B: Applications***, Vol. 22, No. 3, (2009), 291–298.
27. Zakaria, H.M., "Microstructural and corrosion behavior of Al/SiC metal matrix composites", ***Ain Shams Engineering Journal***, Vol. 5, No. 3, (2014), 831–838.
28. Abbass, M.K. and Sultan, B.F., "Effect of Al2O3 nanoparticles on corrosion behavior of aluimnum alloy (Al-4.5 wt% Cu-1.5 wt% Mg) fabricated by powder metallurgy", ***Engineering Structures and Technologies***, Vol. 11, No. 1, (2019), 25–31.
29. Majed, R.A., Mahdi, M., Al-Kaisy, H.A., and Maged, S.A.A., "Corrosion Behavior for Al-Cu-Mg Alloy by Addition SiO2 Particles in Seawater", ***Engineering and Technology Journal, Part (A) Engineering***, Vol. 32, No. 2, (2014), 354–364.
30. Munasir, Triwikantoro1, Zainuri, M., and Darminto, "Synthesis of SiO2 nanopowders containing quartz and cristobalite phases from silica sands", ***Materials Science-Poland***, Vol. 33, No. 1, (2015), 47–55.
31. Munasir, Triwikantoro1, Zainuri, M., Bäßler, R., and Darminto, "Mechanical Strength and Corrosion Rate of Aluminium Composites (Al/SiO2): Nanoparticle Silica (NPS) as Reinforcement", ***Journal of Physical Science***, Vol. 30, No. 1, (2019), 81–97.
32. Mansfeld, F., "Tafel slopes and corrosion rates obtained in the pre-Tafel region of polarization curves", ***Corrosion Science***, Vol. 47, No. 12, (2005), 3178–3186.
33. Oni, B.O., Egiebor, N.O., Ekekwe, N.J., and Chuku, A., "Corrosion behavior of tin-plated carbon steel and aluminum in NaCl solutions using electrochemical impedance spectroscopy", ***ournal of Minerals and Materials Characterization and Engineering***, Vol. 7, No. 4, (2008), 331–346.
34. Gerengi, H., Goksu, H., and Slepski, P., "The inhibition effect of mad Honey on corrosion of 2007-type aluminium alloy in 3.5% NaCl solution", ***Materials Research***, Vol. 17, No. 1, (2013), 255–264.
35. Ihom, A.P., Nyior, G.B. Nor, I.J., Segun, S., and Ogbodo, J., "Evaluation of the corrosion resistance of aluminum alloy matrix/2.5% particulate glass reinforced composite in various media", ***Journal of Science and Technology***, Vol. 1, No. 10, (2012), 560–568.
36. Deepa, P. and Padmalatha, R., "Studies of corrosion of aluminium and 6063 aluminium alloy in phosphoric acid medium", ***International Journal of ChemTech Research***, Vol. 5, No. 6, (2013), 2690–2705.
37. Khavasfar, A., Jafari, A.H., and Moayed, M.H., "An Investigation on the Performance of an Imidazoline Based Commercial Corrosion Inhibitor on CO_2 Corrosion of Mild Steel", ***International Journal of Engineering - Transactions A: Basics***, Vol. 20, No. 1, (2007), 35–44.
38. Azadi, M. and Azadi, M., "Corrosion Failure Study in an Oil Cooler Heat Exchanger in Marine Diesel Engine", ***International Journal of Engineering - Transactions B: Applications***, Vol. 29, No. 11, (2016), 1604–1611.
39. Afzali, P., Yousefpour, M., and Borhani, E., "Effect of deformation-induced defects on the microstructure and pitting corrosion behavior of Al-Ag alloy", ***International Journal of Engineering - Transactions C: Aspects***, Vol. 31, No. 12, (2018), 2092–2101.
40. Salarvand, A., Poursaiedi, E., and Azizpour, A., "Probability Approach for Prediction of Pitting Corrosion Fatigue Life of Custom 450 Steel", ***International Journal of Engineering - Transaction A: Basics***, Vol. 31, No. 10, (2018), 1773–1781.

Corrosion Polarization Behavior of Al-SiO_2 Composites in 1M NaCl and Related Microstructural Analysis

N. Munasir[a], Triwikantoro[b], M. Zainuri[b], R. Bäßler[c], Darminto[b]

[a] *Department of Physics, Faculty of Mathematics and Sciences, Universitas Negeri Surabaya, Jl. Ketintang Surabaya, Indonesia*
[b] *Department of Physics, Faculty of Sciences, Institut Teknologi Sepuluh Nopember (ITS), Surabaya, Indonesia*
[c] *BAM-Federal Institute for Materials Research and Testing, Division 6.2: Corrosion Protection of Technical Plants and Equipment, Unter den Eichen, Berlin, Germany*

P A P E R I N F O

Paper history:
Received 13 February 2019
Received in revised form 29 April 2019
Accepted 03 May 2019

Keywords:
Al-Composite
Corrosion
Corrosion rate
SiO_2 Nanoparticle
Tafel Plot

چکیده

کامپوزیت‌های مرکب از نانوذرات آلومینیم و سیلیکا با افزودن هیدروکسید تترامیلیم آمونیوم (Al-SiO_2 (T)) و بوتانول (Al-SiO_2 (B)) به عنوان مخلوط با موفقیت ساخته شده‌اند. رفتار خوردگی کامپوزیت‌های Al-SiO_2 قبل و بعد از قرار گرفتن در محلول یک مول NaCl با استفاده از قطبش پتانسیودینامیک (تحلیل منحنی Tafel) بررسی شد. این مطالعه همچنین با میکروسکوپ الکترونی روبشی (SEM)، پراکنش انرژی پرتوی ایکس (EDX) و تحقیقات XRD انجام گرفت. قبل از قرار گرفتن در معرض Al-SiO_2(T) بهترین مقاومت در برابر خوردگی را نشان می‌دهد. بهبود عملکرد توسط Al-SiO_2(B) تا ۱۰ برابر بهتر از Al-SiO_2(T) پس از قرار گرفتن در معرض مشاهده شد. افزایش محتوای SiO_2 مقاومت به خوردگی کامپوزیت‌ها را به‌طور قابل توجهی افزایش نمی‌دهد. کامپوزیت Al-SiO_2 با محتوای ۵۰٪ SiO_2 (به‌عنوان ترکیب مطلوب) مقاومت به خوردگی بسیار بالایی را نشان می‌دهد. علاوه بر این، خوردگی حفره‌ای در کامپوزیت‌های Al-SiO_2 دیده می‌شود که نشان‌دهنده‌ی تشکیل محصولات خوردگی در محدوده‌ی دانه است. این محصول توسط حضور SiO_2 در زمینه‌ی آلومینیم و محیط NaCl در دمای ۹۰ درجه‌ی سانتی‌گراد (رویکرد به زمینه‌های ژئوترمال مصنوعی: Na^+، Cl^-، H^+، OH^-) تحت تاثیر قرار گرفت. مطالعه‌ما نشان داد که γ-Al_2O_3، γ-$Al(OH)_3$ و $Al(OH)_2Cl$ محصولات خوردگی غالب هستند.

***doi**: 10.5829/ije.2019.32.07a.11*